entropy

MDPI

Article

Entropy Generation Optimization for Rarified Nanofluid Flows in a Square Cavity with Two Fins at the Hot Wall

Wael Al-Kouz [1,*], Ahmad Al-Muhtady [2], Wahib Owhaib [2], Sameer Al-Dahidi [2], Montasir Hader [3] and Rama Abu-Alghanam [4]

1 Mechatronics Engineering Department, German Jordanian University, Amman 11180, Jordan
2 Mechanical and Maintenance Engineering Department, German Jordanian University, Amman 11180, Jordan; ahmad.almuhtady@gju.edu.jo (A.A.-M.); Wahib.Owhaib@gju.edu.jo (W.O.); Sameer.Aldahidi@gju.edu.jo (S.A.-D.)
3 Aeronautical Engineering Department, Jordan University of Science and Technology, Irbid 22110, Jordan; hader@just.edu.jo
4 Energy Engineering Department, German Jordanian University, Amman 11180, Jordan; rama.abualghanam@gmail.com
* Correspondence: wael.alkouz@gju.edu.jo; Tel.: +962-6429-4444 (ext. 4519)

Received: 6 January 2019; Accepted: 16 January 2019; Published: 22 January 2019

Abstract: Computational Fluid Dynamics (CFD) is utilized to study entropy generation for the rarefied steady state laminar 2-D flow of air-Al_2O_3 nanofluid in a square cavity equipped with two solid fins at the hot wall. Such flows are of great importance in industrial applications, such as the cooling of electronic equipment and nuclear reactors. In this current study, effects of the Knudsen number (Kn), Rayleigh number (Ra) and the nano solid particle's volume fraction (ϕ) on entropy generation were investigated. The values of the parameters considered in this work were as follows: $0 \leq Kn \leq 0.1$, $10^3 \leq Ra \leq 10^6$, $0 \leq \phi \leq 0.2$. The length of the fins (L_F) was considered to be fixed and equal to 0.5 m, whereas the location of the fins with respect to the lower wall (H_F) was set to 0.25 and 0.75 m. Simulations demonstrated that there was an inverse direct effect of Kn on the entropy generation. Moreover, it was found that when Ra was less than 10^4, the entropy generation, due to the flow, increased as ϕ increases. In addition, the entropy generation due to the flow will decrease at Ra greater than 10^4 as ϕ increases. Moreover, the entropy generation due to heat will increase as both the ϕ and Ra increase. In addition, a correlation model of the total entropy generation as a function of all of the investigated parameters in this study was proposed. Finally, an optimization technique was adapted to find out the conditions at which the total entropy generation was minimized.

Keywords: natural convection; entropy generation; square cavity; low pressure; nanofluid

1. Introduction

Unconventional reservoirs have drawn intensive attention recently [1], and fractal-based approaches are key methods used to characterize the pore structure, physical properties, and fluid flow in them under different mechanisms [2–4]. One of the basic problems that has been investigated deeply in the last few decades is the natural convection mode of heat transfer that serves in a number of engineering applications, for example solar collectors [5,6], fuel cell industry [7], petroleum engineering [8,9], and cooling of electronic components [10,11], etc. The unsatisfying heat-transfer rate due to the natural convection, however, is a significant issue for the application. As a result, the dispersion of nano solid particles into a base fluid has been developed as a widely-used method to address such an issue. By dispersing nano solid particles into the base fluid, the resulting nanofluid will

have superior thermal properties compared to the base fluid. For instance, Choi et al. [12] introduced "nanofluids" used in many industrial applications. In the work conducted by Khanafer et al. [13], the numerical solution of natural convection heat transfer in a two-dimensional enclosure where nanofluid is used as the working fluid was analyzed. They concluded that there is a direct proportional relationship between the heat transfer rate and the ϕ at a given Grashof number. Moreover, Khanafer et al. [14] studied the validity of nanofluid's effective viscosity and thermal conductivity models along with experimental results available in the literature and their features in the enhancement of heat transfer. Buongiorno [15] discussed and provided an explanation for the convective heat transfer enhancement associated with using nanofluid. He proposed a new model for the transport phenomena in nanofluids based on a two-component nonhomogeneous equilibrium model. In Oztop et al. [16], Computational Fluid Dynamics (CFD) analysis was used to solve a mathematical model for fluid flow and heat transfer due to buoyancy effect in a partially heated cavity filled with nanofluid. They noticed that at a given *Ra*, there was an enhancement in heat transfer as ϕ increased. In addition, Ghasemi et al. [17] numerically studied the natural convection of water/Al_2O_3 nanofluid in a square cavity under a magnetic field. They found that for any ϕ, heat transfer rate was strongly dependent on *Ra*; it may enhance or deteriorate. Also, Kefayati et al. [18] simulated the heat transfer and flow of free convection in cavities filled with water/SiO_2 using a lattice Boltzmann method. They concluded that there was a direct relationship between the heat transfer rate and ϕ for the studied aspect ratios and *Ra*. Additionally, Kefayati [19] analyzed entropy generation and heat transfer of laminar free convection flow in a porous square cavity filled with non-Newtonian nanofluid Cu/water using a finite difference lattice Boltzmann method. He found that the heat transfer rate was enhanced and entropy generation was dropped when both ϕ and *Ra* were increased. Al-Kouz et al. [20] numerically investigated free convection heat transfer characteristics of rarefied flows in an inclined square enclosure equipped with two solid or porous fins at the hot wall. They found that with equipped fins at the hot wall, the heat transfer rate was enhanced. Moreover, they found that using porous fins had an advanced impact on heat transfer. Al-Kouz et al. [21] numerically studied the low-pressure gaseous flows' free convection heat transfer characteristics of nanofluid (Air/Al_2O_3) inside a square enclosure equipped with two solid fins at the hot wall. They revealed that for a given *Ra*, adding nanoparticles resulted in an enhancement in the heat transfer rate.

Studying the rate of entropy generation is important in engineering because it suitably calculates the irreversibility of thermodynamics. For example, Kefayati et al. [22] analyzed the natural convection flow in an inclined cavity of non-Newtonian nanofluid using Buongiorno's mathematical model by the finite difference lattice Boltzmann method. They observed that the lowest entropy generation and highest Bejan number occur at inclined an angle of zero at a given *Ra*. Parvin et al. [23] numerically investigated entropy generation and laminar free convective heat transfer in an odd-shaped enclosure filled with Cu/water nanofluid. Their results revealed that with increasing *Ra*, entropy generation caused by heat was increased while the entropy generation caused by the fluid flow was decreased. They also extracted the optimum value of *Ra* at which the heat transfer was maximized and the total entropy generation was minimized. In the work of Merji et al. [24] and Mahmoudi et al. [25], numerical study using the lattice Boltzmann method for the laminar free convection and entropy generation in a square enclosure filled with water/Al_2O_3 nanofluid under a magnetic field was conducted. They found that ϕ had a direct effect on the heat transfer rate and an inverse effect on the total entropy generation. In the article by Armaghani et al. [26], a numerical study of the entropy generation and natural convection heat transfer in a baffled L-shaped cavity filled with water-Alumina nanofluid was presented. The authors revealed that as the aspect ratio increased the heat transfer rate enhanced, particularly when nanofluid was utilized as a working fluid. Al-Zamily [27] numerically studied the influence of a porous central layer thickness inside a cavity on heat transfer, fluid flow and entropy generation. The cavity was filled with nanofluid (water/ TiO_2) at a constant wall heat flux located at two different wall positions. Results showed that the nanofluid flow was stronger and heat transfer rate increased as the central porous layer thickness decreased. He also concluded that

the heat transfer rate was enhanced with ϕ. Bouchouch et al. [28] investigated the free convection heat transfer and entropy generation of nanofluid (water/Al_2O_3) in a square enclosure with a thick bottom wall heated with a non-isothermal heater with a sinusoidal function. The authors showed that using the nanofluid enhanced the heat transfer. Moreover, they concluded that the entropy generation increased with *Ra*. Ashorynejad et al. [29] numerically investigated the entropy generation and free convection heat transfer in a square porous enclosure with various porosities filled with different water base nanofluids (Al_2O_3, TiO_2 and CuO) using the lattice Boltzmann method. They concluded that the dispersion of nano solid particles decreased the total entropy generation and enhanced heat transfer. They also concluded that the entropy generation was increased with cavity porosity. In their work, Sheremet et al. [30] numerically studied the free convection heat transfer and entropy generation of water based nanofluid inside a square cavity with variable temperature distribution sidewalls. They concluded that the total entropy generation increased with *Ra* and a rise of the temperature distribution in the sidewalls. Alsabery et al. [31] numerically investigated the free convection and entropy generation of nanofluid (water/Al_2O_3) in a square enclosure with concentric solid inserts at different temperature distributions. They observed a strong heat transfer rate enhancement with increasing *Ra* for a given Rayleigh number range. In addition, they concluded that the total entropy generation rose with increasing *Ra* and with the reduction in the size of the concentric solid insert beyond a given *Ra*. A numerical investigation using the two-phase mixture and Darcy-Birnkman-Forchheimer model for free convection and entropy generation of nanofluid (water/Cu) inside a cavity furnished with porous fins was presented by Siavashi et al. [32]. They revealed that a low ϕ enhanced the heat transfer rate at a given *Ra*. They also found that the thermal irreversibility was dominant pertaining to entropy generation due to friction. Finally, they concluded that the entropy generation was reduced by using porous fins. Kashyap et al. [33] numerically investigated using a two-phase lattice Boltzmann the natural convection of nanofluid (water/Cu) in a porous square cavity at different boundary conditions. They observed that for all the boundary conditions they studied, the use of nanofluid enhancesd the heat transfer and reduced the entropy generation depending on ϕ. Gibanov et al. [34] analyzed numerically the free convection heat transfer and entropy generation of nanofluid (water/Alumina) in a lid-driven cavity with a bottom solid wall. They concluded that ϕ had a direct effect on the heat transfer. Mansour et al. [35] numerically investigated the entropy generation and magneto-hydrodynamics (MHD) natural convection heat transfer in a square porous enclosure filled with hybrid nanofluid (water/Cu/Al_2O_3). They revealed that for a given *Ra*, the heat transfer rate was decreased and the entropy generation was increased with increasing ϕ. Rahimi et al. [36] investigated natural convection heat transfer and the entropy generation of nanofluid (water/CuO) inside a square cavity equipped with fins. They concluded that the heat transfer rate increased with increasing *Ra* and ϕ, whereas entropy generation increased with *Ra* and decreased with ϕ for the investigated parameters ranges. In their paper, Rashidi et al. [37] investigated the effects of different modeling approaches on the entropy generation in a circular tube heat exchanger using nanofluids, where the considered geometry was a horizontal tube with a constant wall heat flux. The flow regime was turbulent. They found out that the values for entropy generation were very close for the single phase and mixture models. Additionally, they concluded that for the higher volume fractions (i.e., greater than 4%), differences between the models appeared. In their work, Yarmand et al. [38], numerically studied the entropy generation during turbulent flow of Zirconia/water and other nanofluids in a square cross section tube with a constant heat flux, where the flow was assumed to be turbulent. Their results showed that with the optimal volume concentration of nanoparticles minimized, the entropy generation increased when Reynolds number decreased. It was also found that the thermal entropy generation increased with the increase of the nanoparticle size, whereas the frictional entropy generation decreased. Entropy generation in the thermal radiative loading of structures with distinct heaters has been studied numerically by Jamalabadi et al. [39]. They used a finite volume analysis and the semi implicit method for pressure linked equations to solve for the continuity, momentum and energy equations, and their results showed that the entropy value was

more influenced by the temperature than the density. They also showed that the heating ratio of the onset of natural and radiative entropy generation increased by an increase of number of discrete heater sources. In their research, Aghaei et al. [40] experimentally and numerically analyzed the effect of horizontal and vertical elliptic baffles inside an enclosure on the mixed convection of a MWCNTs-water nanofluid and its entropy generation, and they concluded that the horizontal placement of a thermal baffle led to a higher heat transfer rate. Moreover, they found that the entropy generation values in the horizontal position were higher than the vertical position. Mahmoudinezhad et al. [41] numerically and experimentally investigated the adiabatic partition effect on the natural convection heat transfer inside a square cavity, where the flow was considered to be steady state, 2-D. They used a finite volume analysis along with the Mach–Zehender interferometer to carry out the study. Their results showed that the average Nusselt number increased with an increasing Rayleigh number. However, for a given *Ra*, the maximum and minimum heat transfer occurred at the partition angles of 45° and 90°, respectively. Finally, Nasiri et al. [42] used a smoothed particle hydrodynamics approach to investigate the forced convection nanofluid heat transfer over a horizontal cylinder. Their results show that the smoothed particle hydrodynamics approach was the appropriate method for such numerical modeling. In addition, they concluded that the nanofluid heat transfer characteristics had marked improvements compared to base fluids.

Despite many studies in the field of entropy generation dealing with water-based nanofluid inside square cavities, there is a lack in studies that tackle the entropy generation of natural convection low-pressure cavities filled with an air based nanofluid. Therefore, the purpose of the present numerical investigation is to give more insight into the entropy generation in square cavities equipped with two solid fins at the hot wall filled with low-pressure air/Al_2O_3 nanofluid. Analyzed parameters include the Rayleigh number ($10^3 \leq Ra \leq 10^6$) to cover both the conduction dominant and convection dominant modes of heat transfer, the Knudsen number ($0 \leq Kn \leq 0.1$) to cover both the slip and continuum flow regimes, and the nanosolid particles volume fraction ($0 \leq \phi \leq 0.2$).

2. Mathematical Modeling

2.1. Mathematical Formulation

In this study, a two-dimensional steady state laminar natural convection of air/Al_2O_3 nanofluid flow was investigated. Due to a small temperature difference between the hot and cold walls, all of the thermophysical properties of the nanofluid were assumed constant except for the density variation that was modeled using the Boussinesq approximation. Figure 1 represents the geometry of a square cavity of length *L* with two fins at the hot wall. h_1 represents the position of the lower fin relative to the lower wall while h_2 represents the upper fin position relative to the lower wall. In the current investigation, both slip and continuum flow regimes were analyzed.

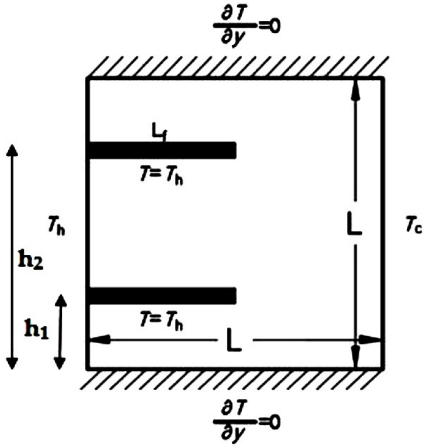

Figure 1. The configuration used for the computational domain.

Dispersing nanoparticles to the base fluid will enhance the thermophysical properties of the resulting nanofluid. As reported in Al-Kouz et al. [21], these properties can be calculated based on the following equations:

Viscosity:

$$\mu_{nf} = \frac{\mu_f}{(1-\varnothing)^{2.5}} \tag{1}$$

Density:

$$\rho_{nf} = (1-\varnothing)\rho_f + \varnothing\rho_s \tag{2}$$

Heat Capacitance:

$$C_{P_{nf}} = (1-\varnothing)(C_P)_f + \varnothing(C_P)_s \tag{3}$$

Thermal Expansion Coefficient:

$$\beta_{nf} = \beta_f \left[\frac{1}{1+\frac{(1-\varnothing)\rho_f}{\varnothing\rho_s}} \frac{\beta_s}{\beta_f} + \frac{1}{1+\frac{\varnothing}{1-\varnothing}\frac{\rho_s}{\rho_f}} \right] \tag{4}$$

Thermal Conductivity:

$$k_{nf} = k_f \frac{k_s + 2k_f - 2\varnothing\left(k_f - k_s\right)}{k_s + 2k_f + \varnothing\left(k_f - k_s\right)} \tag{5}$$

Table 1 shows the thermophysical properties utilized to obtain the resulting properties of the Al_2O_3-air nanofluid.

Table 1. Thermophysical properties of air and Al_2O_3.

Physical Properties	Air	Al_2O_3
Cp (J/kg·K)	1006.43	765
ρ (kg/m^3)	1	3970
k (W/m^2·K)	0.025	40
β (1/K)	0.00333	0.0000085
α (m^2/s)	0.000019	0.00001317

The governing equations of the current study are reported in Al-Kouz et al. [21] and are summarized below:

Continuity:

$$\frac{\partial u}{\partial x} + \frac{\partial v}{\partial y} = 0 \tag{6}$$

x-momentum:

$$\rho_{nf}\left(u\frac{\partial u}{\partial x} + v\frac{\partial u}{\partial y}\right) = -\frac{\partial P}{\partial x} + \mu\left(\frac{\partial^2 u}{\partial x^2} + \frac{\partial^2 u}{\partial y^2}\right) \tag{7}$$

y-momentum:

$$\rho_{nf}\left(u\frac{\partial v}{\partial x} + v\frac{\partial v}{\partial y}\right) = -\frac{\partial P}{\partial y} - \rho_{nf}g + \mu\left(\frac{\partial^2 v}{\partial x^2} + \frac{\partial^2 v}{\partial y^2}\right) \tag{8}$$

Energy:

$$\rho_{nf}C_{p_{nf}}\left(u\frac{\partial T}{\partial x} + v\frac{\partial T}{\partial y}\right) = k_{nf}\left(\frac{\partial^2 T}{\partial x^2} + \frac{\partial^2 T}{\partial y^2}\right) \tag{9}$$

With the following boundary conditions in the slip flow regime as reported in Karniadakis et al. [43], Lockerby et al. [44] and Colin [45]:

$$u_w - u_g = \left(\frac{2-\sigma_v}{\sigma_v}\right)\lambda\frac{\partial u}{\partial n} \approx \left(\frac{2-\sigma_v}{\sigma_v}\right)K_n\left(u_g - u_c\right) \tag{10}$$

$$v_g = 0 \tag{11}$$

$$T_w - T_g = \left(\frac{2-\sigma_T}{\sigma_T}\right)\frac{2\gamma}{\gamma+1}\frac{k}{\mu c_v}\lambda\frac{\partial T}{\partial n} \approx \left(\frac{2-\sigma_T}{\sigma_T}\right)\frac{2\gamma}{\gamma+1}\frac{k}{\mu c_v}(T_g - T_c) \tag{12}$$

In Equations (10) and (12), σ_v and σ_T refer to the momentum and thermal accommodation coefficients, respectively, and Kn is defined as:

$$K_n = \frac{\lambda}{L} \tag{13}$$

where L is the square cavity characteristic length and λ is the mean free path.

The imposed thermal boundary conditions at x = 0 and L:

$$At(x = 0, y),\ T = T_h \tag{14}$$

$$At(x = L, y),\ T = T_c \tag{15}$$

where T_h is the temperature at the hot surface and T_c is the temperature at the cold surface. The temperature of the fins was set to T_h

The local heat fluxes could be calculated by Equations (16) and (17) as reported by [21]:

$$q''_F = -k\frac{\partial T}{\partial n}\bigg|_F \tag{16}$$

$$q''_h = -k\frac{\partial T}{\partial n}\bigg|_h, q''_c = -k\frac{\partial T}{\partial n}\bigg|_c \tag{17}$$

To calculate the total heat transfer from the hot to the cold wall, one could integrate the local heat flux along the wall of the hot wall combined with the fins as follows:

$$Q = \sum\left(\int_{A_h} q''_h dA_h + \int_{A_F} q''_F dA_F\right) = \int_{A_c} q''_c dA_c \tag{18}$$

Then, the average heat transfer coefficient along the combined hot wall and the fins or along the cold surface was derived as follows:

$$\overline{h} = \frac{Q}{(T_i - T_o)A_T} = \frac{Q}{(T_i - T_o)A_c} \tag{19}$$

From the previous equation, one could derive the average Nusselt number for L = 1 m, where:

$$Nu = \frac{\overline{h}L}{k_{n_f}} = \frac{\overline{h}}{k_{nf}} \tag{20}$$

Following Parvin et al. [20], the total entropy generation is defined as:

$$Sgen_{tot} = Sgen_f + Sgen_h \tag{21}$$

In Equation (21), $Sgen_f$ is the entropy generation caused by the flow and $Sgen_h$ is the entropy generation due to heat, where,

$$Sgen_f = \frac{k_{nf}}{{T_o}^2}\left[\left(\frac{\partial T}{\partial x}\right)^2 + \left(\frac{\partial T}{\partial y}\right)^2\right] \tag{22}$$

$$Sgen_h = \frac{\mu_{nf}}{T_o}\left[2\left(\frac{\partial u}{\partial x}\right)^2 + 2\left(\frac{\partial v}{\partial y}\right)^2 + \left(\frac{\partial u}{\partial x} + \frac{\partial v}{\partial y}\right)\right] \text{ and } T_o = \frac{T_h + T_c}{2} \tag{23}$$

2.2. Numerical Solution

In this study, a finite volume technique was utilized using ANSYS Fluent software (Version 18, ANSYS, Inc., South pointe, PA, USA) to investigate the flow, heat transfer characteristics and the total entropy generation for steady, 2-D, laminar natural convection rarefied nanofluid in a square cavity. The SIMPLE algorithm presented by Versteeg and Malalasekera [46] and Patankar and Spalding [47] was utilized. In order to calculate the pressure field, the PRESTO algorithm was used. Moreover, a hybrid second order accuracy scheme of upwind and central difference was used to differentiate the convective terms. As a starting point, 40 × 40 mesh elements were tested. In addition, σ_v and σ_T for all simulations were considered to be in unity. The solution was converged when the maximum of the normalized absolute residual across all nodes was $<10^{-6}$.

2.3. Grid Independency

The grid that was used in all simulations was a two dimensional mesh, which is shown in Figure 2. Initially, the step sizes of the grid were increasing in the x and y directions with expansion factors of 1.06 and 1.15 respectively, these values were selected to capture the gradient's near solid-fluid interface. Then the mesh was adapted and the velocity gradients near the solid surfaces were calculated. After this, the number of cells was increased to lower the gradients below a certain value. It was noticed that any further change in these parameters would not affect the results. A grid independency test was performed by monitoring *Nu* at the cold surface, and solutions for different numbers of grid nodes were obtained. It was obvious that adding more cells beyond a certain value would not affect *Nu*. In addition, the average magnitude of the velocity inside the cavity was monitored and tabulated. Table 2 summarizes the values of *Nu* as well as the velocity magnitude inside the cavity, along with their relative error to the values obtained for a mesh size of 100 × 100 elements.

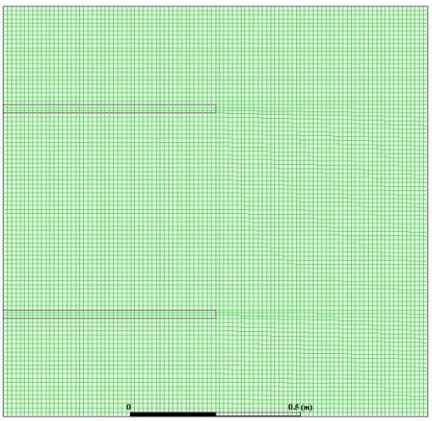

Figure 2. 2D mesh utilized in all simulations.

Table 2. Mesh independency test.

Mesh Size	Average Velocity (m/s)	Relative Error in the Average Velocity (%)	*Nu*	Relative Error in *Nu* (%)	Simulation Time (s)
40 × 40	0.00055464421	0.050516	5.0973	0.044250507	415
60 × 60	0.00057143194	0.021778	4.9694	0.01804847	622
80 × 80	0.00057617336	0.013661	4.9157	0.00704730	739
100 × 100	0.00058415352	0.0	4.8813	0.0	823
120 × 120	0.00058415352	0.0	4.881297	6.15×10^{-7}	876

Figure 3 and Table 2 demonstrate that the solution was converged for the 100 × 100 nodes grid size. This grid size was considered for all simulations conducted in this study.

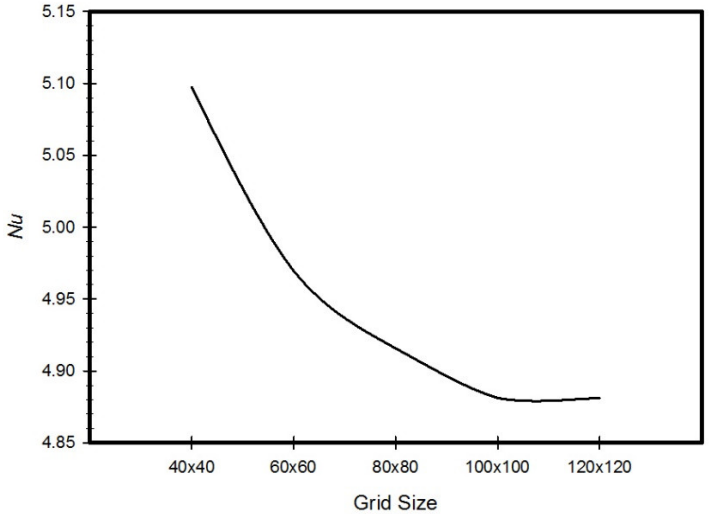

Figure 3. Grid independency test for Nusselt number.

2.4. Code Verification

For verification purposes, results of the current code were compared with the results extracted by Parvin et al. [23] for the case of an odd shaped enclosure filled with Cu/water nanofluid. Figure 4 illustrates a satisfying agreement of our proposed model and the model obtained by Parvin et al. [23] at $\phi = 5\%$.

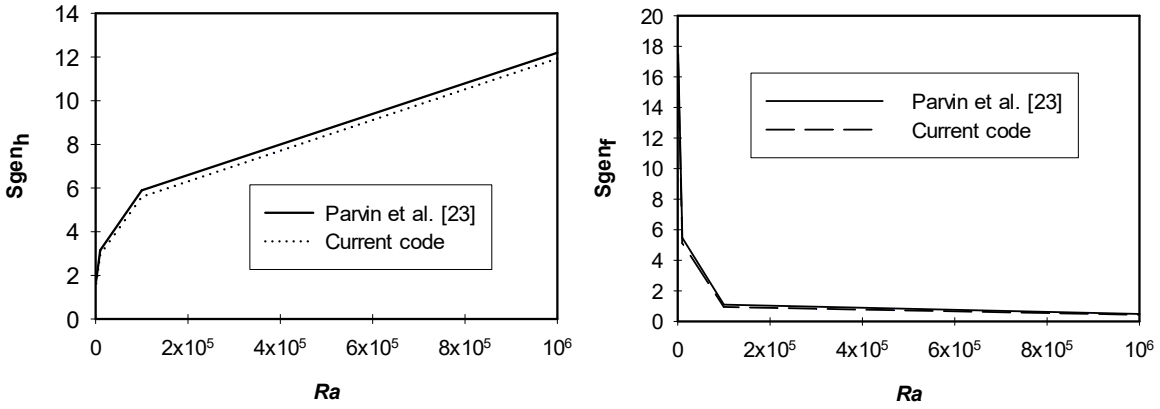

Figure 4. Validation of the current code.

3. Results and Discussion

Figures 5–7 show the total entropy generation contours inside the square cavities with a fin position of $H_F = 0.25$, 0.75 m and fin lengths of 0.5 m for the cases where $Kn = 0$, 0.05 and 0.1 to cover both the slip and continuum flow regimes. Moreover, $\phi = 0$, 0.01, 0.1 and 0.2 were considered. The contours were plotted for cases where $Ra = 10^3$, 10^4 and 10^5. It was clear from the contours that there was a formation of a large clockwise rotating cell. By increasing Kn for the same ϕ and Ra, less circulation is observed inside the cavity. This decrease will affect the heat transfer characteristics. For the cases of $\phi = 0.2$ and different Kn, more distortion to the flow was observed compared to the other values of ϕ. More recirculation and distorted contours lead to better heat transfer enhancement. Moreover, figures showed that as Ra increased for the same Kn and ϕ, more distortion of the contours occurred inside the cavity, and hence entropy generation increased as a consequence to the increase in the velocity gradients. But still the entropy generation caused by heat was dominant.

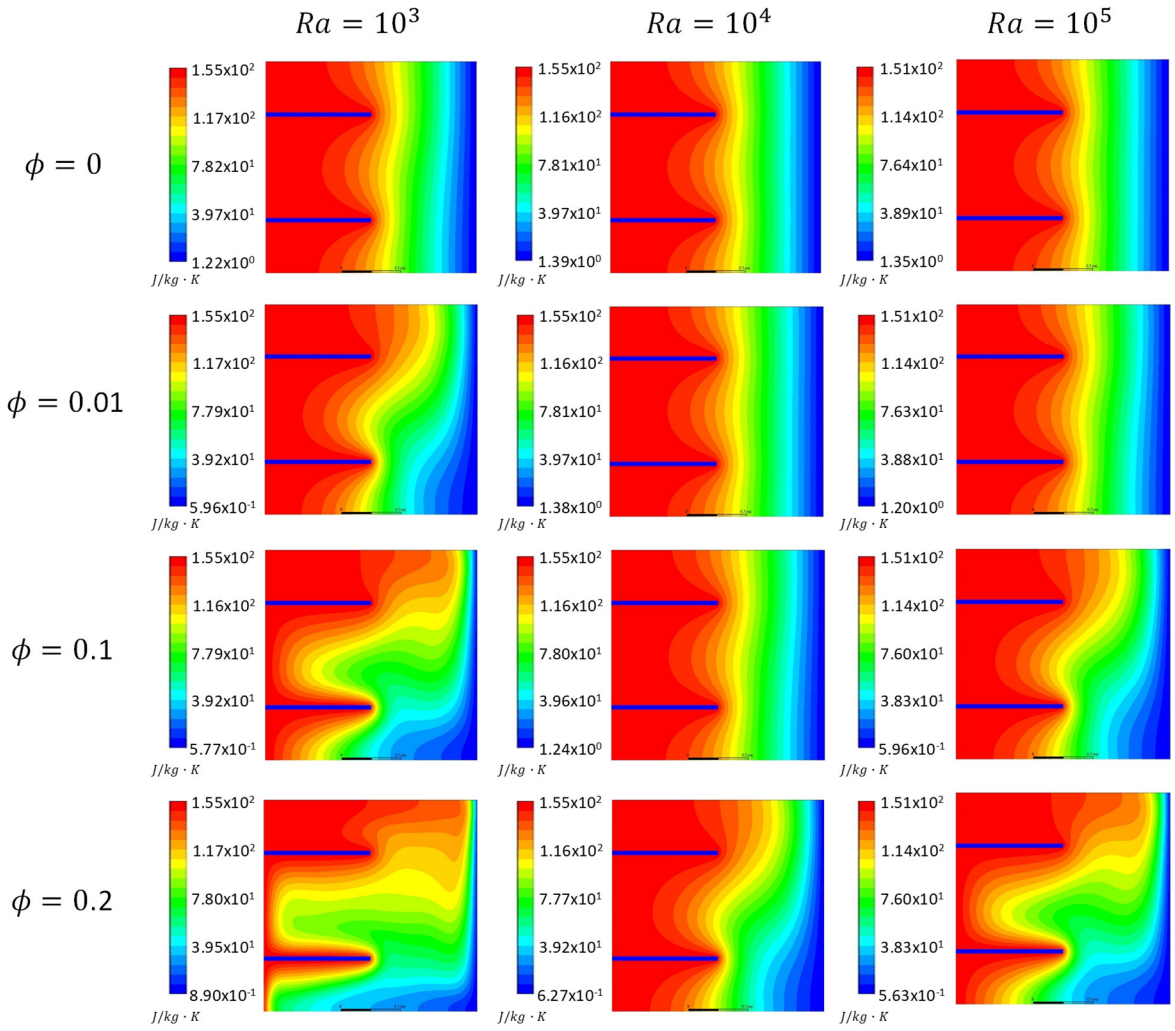

Figure 5. Total entropy generation contours, Kn = 0 at different nanoparticles volume fractions (ϕ = 0, 0.01, 0.1 and 0.2) and $Ra = 10^3$, 10^4 and 10^5.

Figure 8 illustrates variations in entropy generation caused by heat for different nano solid particles volume fractions at different Kn values for the cases of Ra = 1000 and 10,000. The graphs show that for the two values of Ra, as the ϕ increased the entropy generation due to heat increased as well. This could be attributed to the fact that at a low Ra, the dominant mode of heat transfer was conduction, and by adding nano solid particles, k_{eff} would increase and a better heat transfer was achieved. Better heat transfer implied that the increase in the entropy generation resulted from heat. Moreover, the graphs showed that as Kn increased for the same ϕ, the entropy generation due to heat decreased. Higher Kn resulted in more rarefaction effects and consequently less interaction between the nanofluid particles, which lead to less entropy generation. Finally, the graphs also showed that for the higher Ra, the entropy generation due to heat increased for the same values of Kn and the nano solid particles volume fraction. In Figures 5–8, as Ra increased, convection became the dominant mode of heat transfer leading to greater circulation of the flow, and consequently an increase in the total entropy generation was observed.

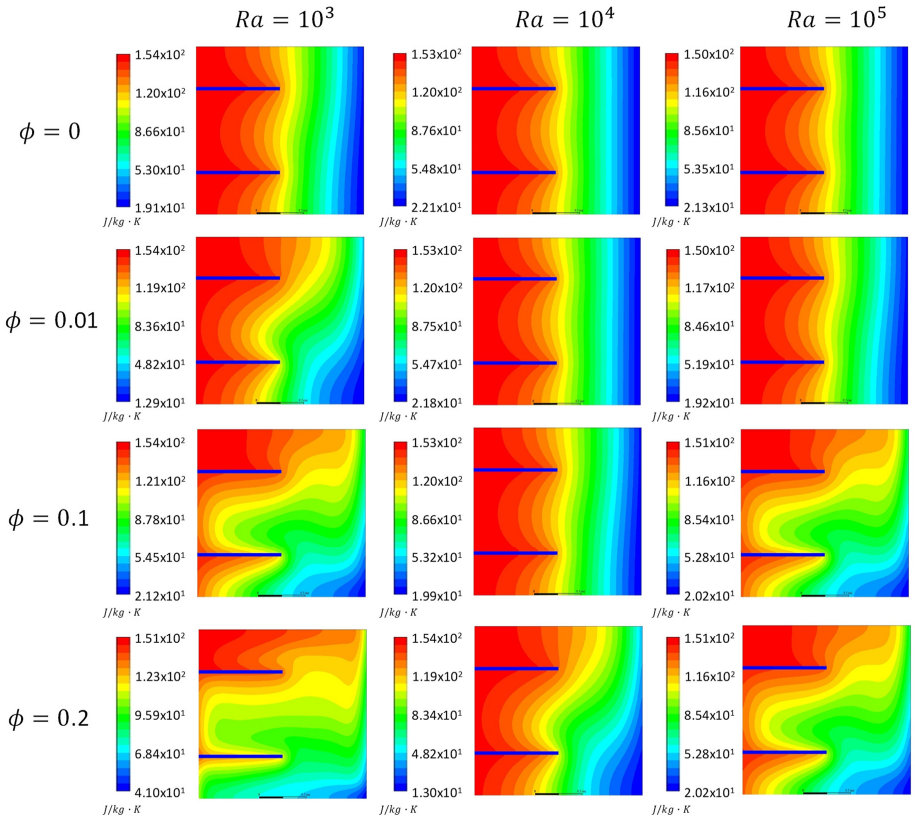

Figure 6. Total entropy generation contours, Kn = 0.05 at different nanoparticles volume fractions (ϕ = 0, 0.01, 0.1 and 0.2) and $Ra = 10^3$, 10^4 and 10^5.

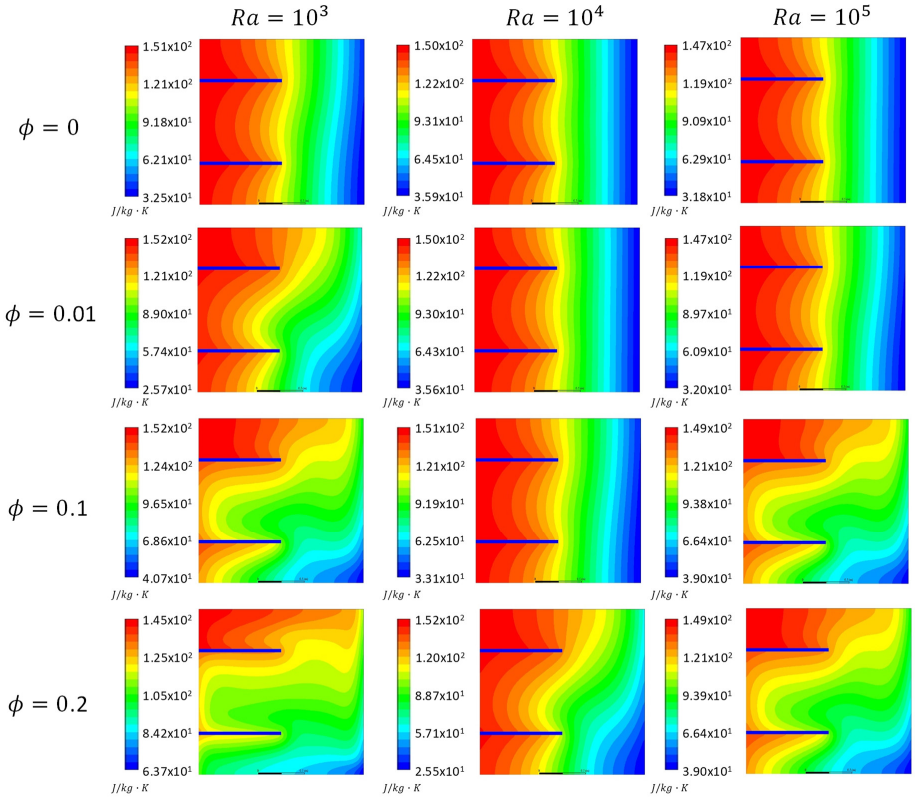

Figure 7. Total entropy generation contours, Kn = 0.1 at different nanoparticles volume fractions (ϕ = 0, 0.01, 0.1 and 0.2) and $Ra = 10^3$, 10^4 and 10^5.

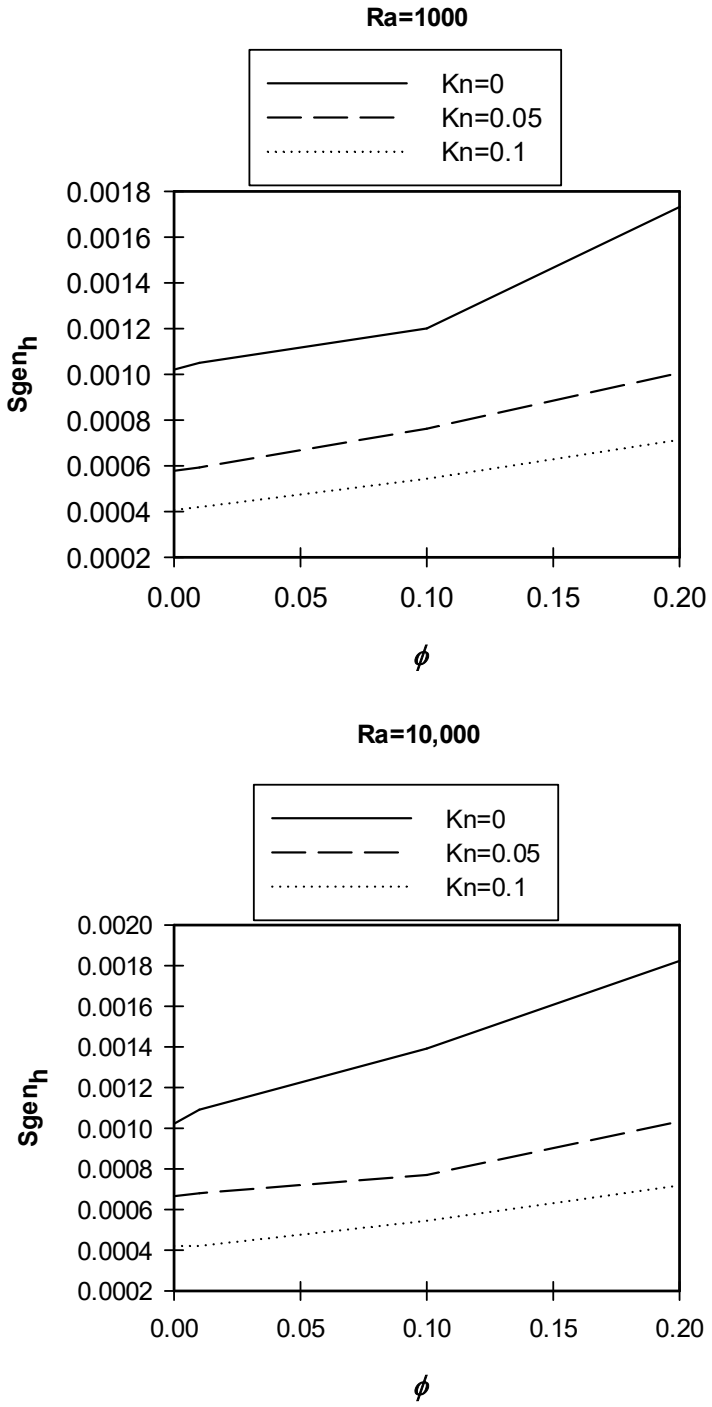

Figure 8. Variation of $Sgen_h$ with φ at different Kn, Ra = 1000, 10,000.

Figure 9 shows variations of the entropy generation due to heat for different nano solid particles volume fractions at different Kn for the cases of $Ra = 10^5$ and 10^6. The graphs show that for the two values of Ra, as the ϕ increased the entropy generation caused by heat decreased. This was mainly because at high Ra, the dominant mode of heat transfer was convection, and by adding nano solid particles, the lowering effect of nano solid particles on convection heat transfer became dominant. Moreover, the graphs show that a higher Kn would result in less entropy generation. Finally, the graphs also show that for the higher Ra, the entropy generation as a result of heat increased for the same value of Kn and ϕ.

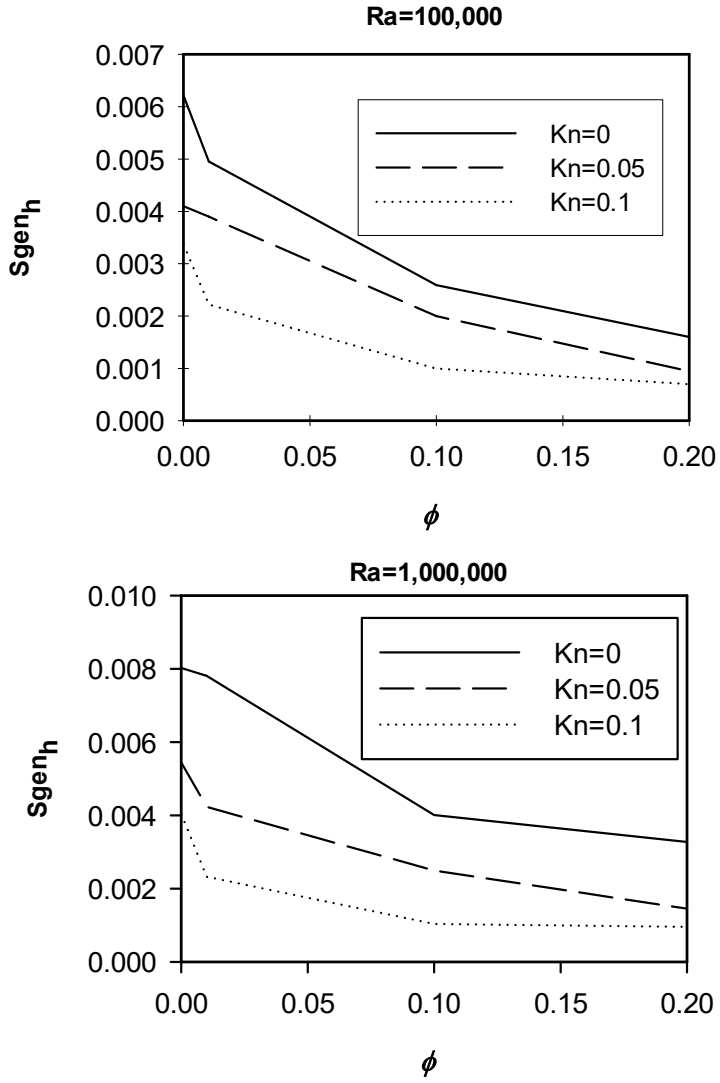

Figure 9. Variation of $Sgen_h$ with ϕ at different Kn, Ra = 100,000, 1,000,000.

Variations of the entropy generation attributable to the flow with Ra at different values of nano solid particles volume fractions are plotted in Figure 10. The graph shows that as Ra increased, the entropy generation by reason of the flow would increase. As Ra increased, more circulation occurred inside the cavity, which resulted in an increase in both velocity gradient and entropy generation. Moreover, as Kn increased, the entropy generation due to flow would decrease, as a result of the rarefaction effects. Finally, as the nano solid particles volume fraction increased, the entropy generation increased because of the flow (friction) effects.

Based on the simulation results, a correlation of the entropy generation among all parameters considered in this study with $R^2 = 0.92$ was presented as follows:

$$S_{gen,tot} = C_1 C_2^{Kn} Ra^{C_3} C_4^{\phi} \tag{24}$$

where, $C_1 = 2.2 \times 10^{-4}$ kJ/kg·K, $C_2 = 0.134$, $C_3 = 0.226$, $C_4 = 0.0077$.

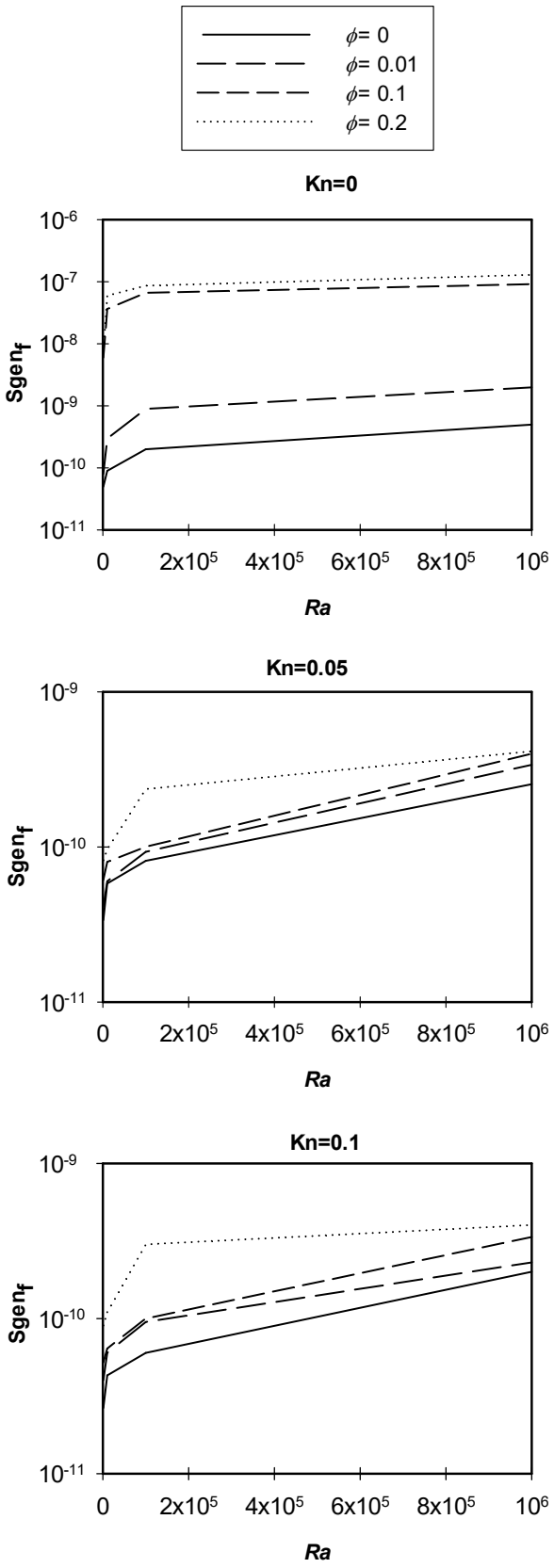

Figure 10. Variation of $Sgen_f$ with Ra at different φ, Kn = 0, 0.05 and 0.1.

It is obvious that the Bejan number was close to unity for all simulations conducted in the study. The Bejan number (Be) is defined as follows:

$$Be = \frac{Sgen_h}{Sgen_{tot}} \tag{25}$$

Figure 11 shows a comparison between the total entropy generation results obtained from the simulations with those obtained from the correlations, the figure shows that there was a great match between the simulation and the correlation results. Deviations between the two were noticed for the conditions at which $Kn = 0$ and $\phi = 0$.

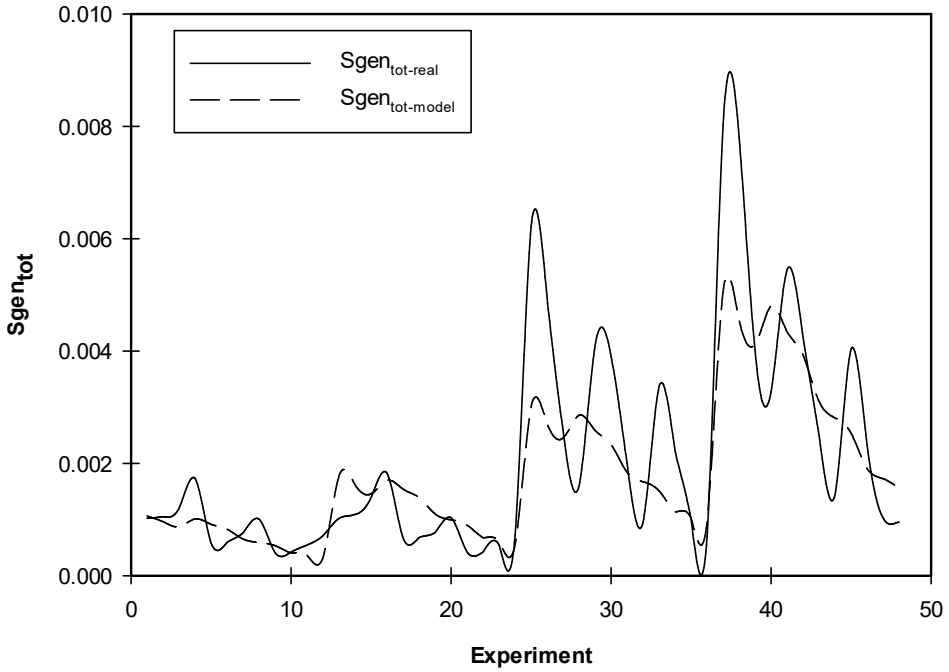

Figure 11. Comparison between the $Sgen_{tot}$ obtained by simulations and those obtained by correlations.

Using Minitab software (Version 18, minitab, State college, PA, USA), the design of experiments for the simulations conducted in this work is shown in Figures 12–15. Figure 12 shows the main effects of Kn, Ra and ϕ on the entropy generation due to heat. It was clear from the figure that there was a strong direct proportional relationship between $Sgen_h$ and Ra higher than 10^4, and a weak proportional relationship for Ra less than 10^4. The graph also shows that there was a weak inverse proportional relationship between $Sgen_h$ and Kn. Moreover, the graph shows a strong inverse proportional relationship between $Sgen_h$ and ϕ.

Figure 13 shows the interaction plots between parameters investigated in this work on $Sgen_h$, and the graph shows that there was an interaction between Ra and ϕ, as they intersect. The changes that we were getting at the level of one independent variable was not changing systematically across the levels of the other independent variable. Therefore, a special effect was achieved when combining them, which was in harmony with the opposite trends seen in Figures 8 and 9.

Figure 14 shows the main effects of (Kn, Ra and ϕ) on the entropy generation due to flow, and it is clear from the figure that there was a strong direct proportional relationship between $Sgen_f$ and Ra. The graph also shows that there was a strong inverse proportional relationship between $Sgen_f$ and Kn values less than 0.05. For Kn values greater than 0.05, there was no effect on $Sgen_f$. Moreover, the graph shows a strong direct proportional relationship between $Sgen_f$ and the volume fraction of the nano solid particles for volume fractions greater than 0.01, and there was almost negligible effect for volume fractions less than 0.01.

Figure 15 illustrates the interaction plots between parameters investigated in this work on $Sgen_f$, the graph shows that there was an interaction between any two parameters, as they do intersect.

Finally, in order to find the conditions at which the minimum entropy generation was obtained, an optimization of the multi variable function of the total entropy generation for the parameter ranges considered in the study was conducted. The optimization that yielded the minimum total entropy generation revealed that this would happen at $Ra = 1001.1$, $\phi = 0.19995$ and $Kn = 0.099$ with minimum total entropy generation of 3.29×10^{-4} kJ/kg·K.

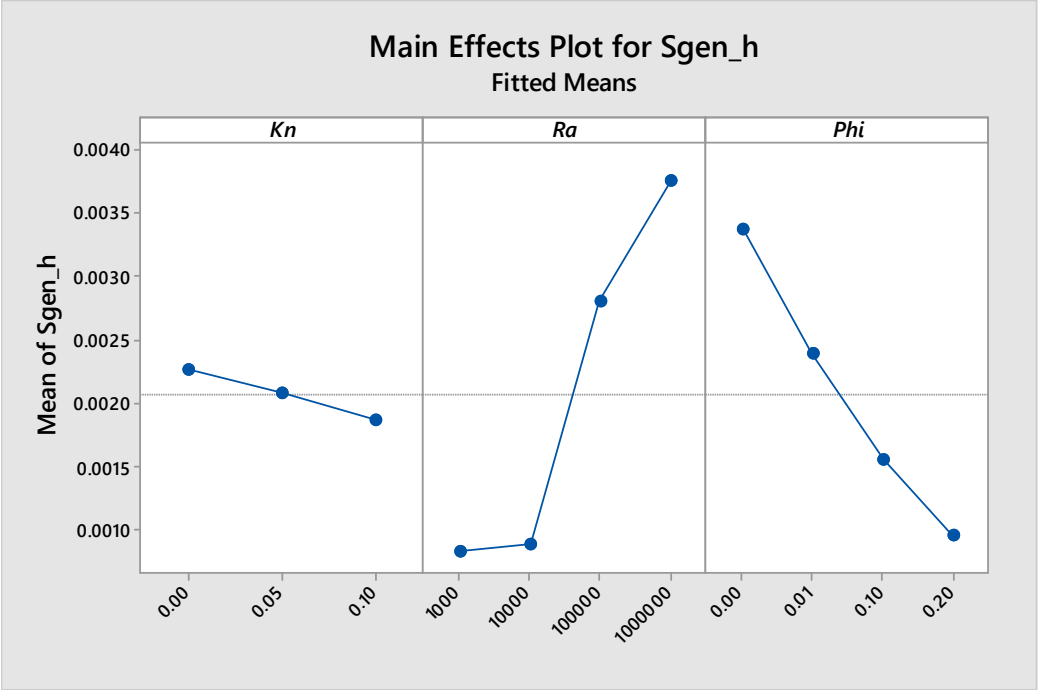

Figure 12. Main effects plot for $Sgen_h$ vs. Kn, Ra and ϕ.

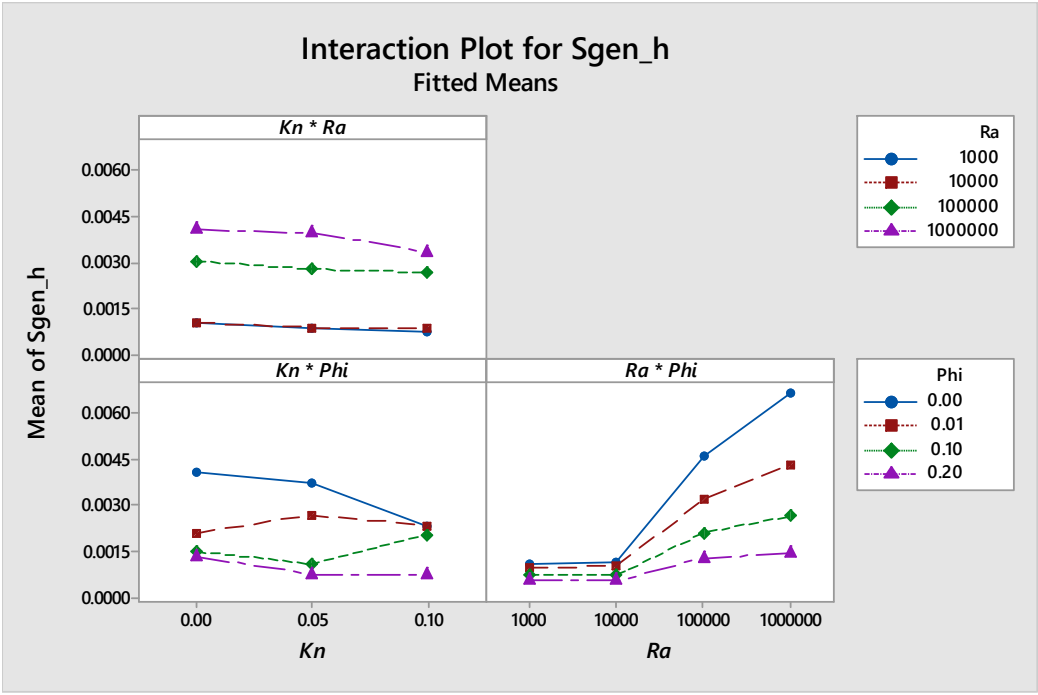

Figure 13. Interaction plot for $Sgen_h$.

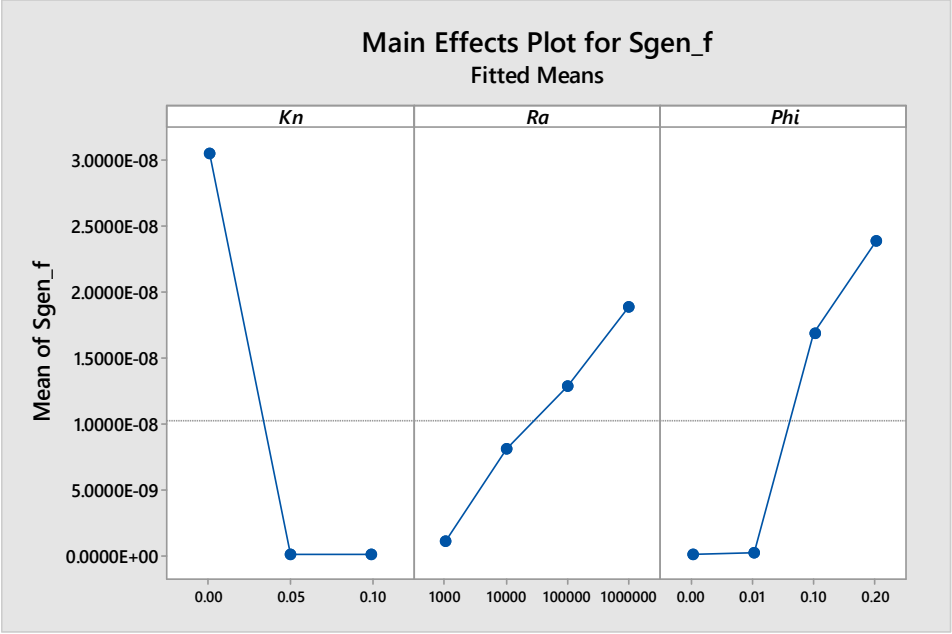

Figure 14. Main effects plot for $Sgen_f$ vs. Kn, Ra and ϕ.

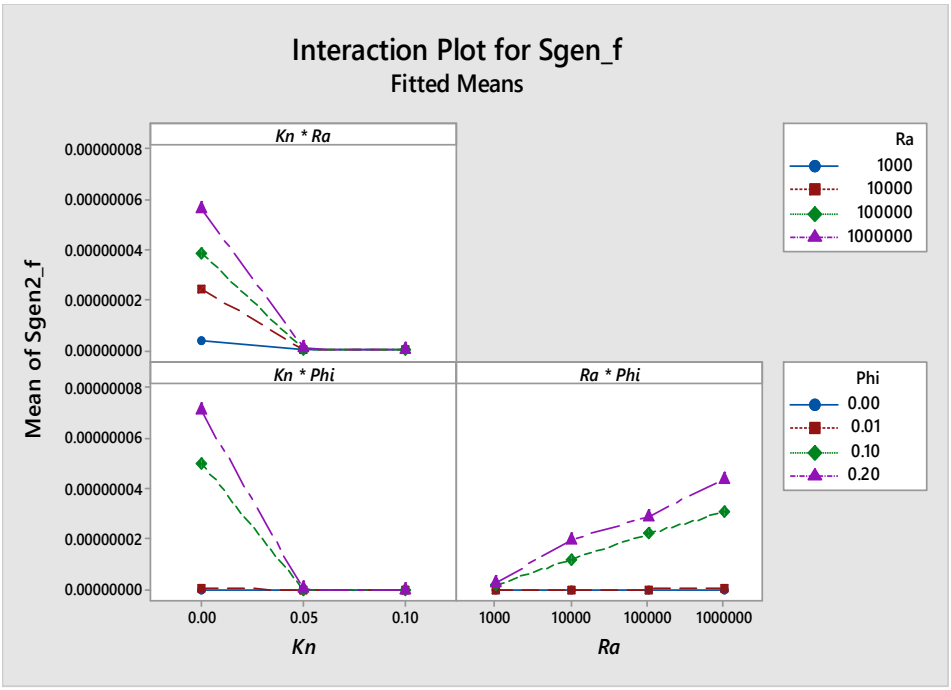

Figure 15. Interaction plot for $Sgen_f$.

It is worth mentioning here that another simulation with the resulting conditions for the minimal entropy generation obtained from the optimization was carried out and the total entropy generation was calculated and was equal to 3.2645×10^{-4} kJ/kg·K, which makes the optimal value extracted from the optimization of the model's correlation in great agreement with the experimental simulation value.

4. Conclusions

Entropy generation analysis using CFD for a steady state, two-dimensional low-pressure gaseous laminar nanofluid flow inside a square cavity equipped with two solid fins attached to the hot wall

was carried out. Such flows are of great importance due to their engineering applications. Rarefaction, Ra and ϕ effects on entropy generation were investigated. Results showed that:

1. As Kn increased, entropy generation decreased.
2. For low Ra numbers, the entropy generation due to flow increased as ϕ increased.
3. For higher Ra, the entropy generation due to flow decreased as ϕ increased.
4. The entropy generation due to heat increased as both Ra and ϕ increase.
5. A correlation model of the total entropy generation as a function of all the parameters investigated in this study was proposed.
6. The conditions for the optimum (minimum) entropy generation in the investigated ranges of the parameters in this study were calculated mathematically and were validated numerically using CFD.

Author Contributions: Conceptualization, W.A.-K. and A.A.-M.; methodology, W.A.-K.; software, R.A.-A.; validation, W.O. and S.A.-D.; formal analysis, W.A.-K. and A.A.-M.; design of experiments, A.A.-M.; correlations, M.H.; writing-original draft preparation, W.A.-K.; writing-review and editing, W.A.-K. and W.O.; supervision, W.A.-K.; project administration, W.A.-K.

Funding: This work results from partial support by the German Jordanian University seed grant under Grant No. SATS 30/2016.

Conflicts of Interest: The authors declare no conflict of interest.

Nomenclature

The following notations are used in this manuscript:

Notations

A_c	Cold wall area (m^2)
A_h	Hot wall area (m^2)
A_F	Fin area (m^2)
Be	Bejan number
C_p	Specific heat ($J{\cdot}kg^{-1}{\cdot}K^{-1}$)
G	Gravity acceleration in the x direction (m/s^2)
h_1	Fin 1 Position (m)
h_2	Fin 2 Position (m)
h	Convection heat transfer coefficient
K	Thermal conductivity ($W{\cdot}m^{-1}{\cdot}K^{-1}$)
Kn	Knudsen number
k_f	Fluid thermal conductivity ($W{\cdot}m^{-1}{\cdot}K^{-1}$)
k_{nf}	Nanofluid thermal conductivity ($W{\cdot}m^{-1}{\cdot}K^{-1}$)
k_s	Nano particles thermal conductivity ($W{\cdot}m^{-1}{\cdot}K^{-1}$)
L	Length of the square cavity (m)
L_F	Fin length (m)
Nu	Nusselt Number
P	Pressure (Pa)
Q	Heat transfer (W)
q''_c	Local heat flux at the wall of the cold surface (W/m^2)
q''_h	Local heat flux at the wall of the hot surface (W/m^2)
q''_F	Local heat flux at the fin (W/m^2)
R	Universal gas constant ($J/mol{\cdot}K$)
Ra	Rayleigh number ($g\beta(T_1\text{-}T_2)L3/\alpha\nu$)
T	Temperature (°C)
T_c	Temperature of the first cell from the wall (°C)
T_i	Hot surface temperature (°C)

Notations

T_o	Cold surface temperature (°C)
T_g	Temperature of the nanofluid (°C)
T_w	Temperature of the wall (°C)
u	Velocity in x-direction (m/s)
u_c	Tangential velocity of the first cell from the wall (m/s)
u_g	Tangential velocity of the nanofluid (m/s)
u_w	Tangential velocity of the wall (m/s)
V	Velocity in y-direction (m/s)
x, y	Cartesian coordinates [m]

Greek Symbols

α	Thermal diffusivity (m^2/s)
β	Thermal expansion coefficient (1/K)
γ	Specific weight (N/m^3)
λ	Molecular mean free path (m)
μ	Dynamic viscosity ($kg{\cdot}m^{-1}{\cdot}s^{-1}$)
ν	Kinematic viscosity ($m^2{\cdot}s^{-1}$)
ϕ	Nano particles volume fraction (%)
ρ	Density of air, given by ideal gas equation (P/RT), (Kg/m^3)
σ_T	Thermal accommodation coefficient
σ_v	Momentum accommodation coefficient

Subscripts

Eff	Effective
f	Fluid
F	Fin
g	Gas flow
i	Hot wall
n	Normal
nf	Nanofluid
o	Cold wall
r	Ratio
w	Wall

References

1. Cai, J.; Zhang, L.; Ju, Y.; Pia, G.; Zhang, Z. An Introduction to Fractal-Based Approaches in Unconventional Reservoirs—Part I. *Fractals* **2018**, *26*, 1802001. [CrossRef]
2. Xiao, B.; Zhang, X.; Wang, W.; Long, G.; Chen, H.; Kang, H.; Ren, W. A Fractal Model for Water Flow through Unsaturated Porous Rocks. *Fractals* **2018**, *26*, 1840015. [CrossRef]
3. Xiao, B.; Chen, H.; Xiao, S.; Cai, J. Research on Relative Permeability of Nanofibers with Capillary Pressure Effect by Means of Fractal-Monte Carlo Technique. *J. Nanosci. Nanotechnol.* **2017**, *17*, 6811–6817. [CrossRef]
4. Xiao, B.; Wang, W.; Fan, J.; Chen, H.; Hu, X.; Zhao, D.; Zhang, X.; Ren, W. Optimization of the Fractal-Like Architecture of Porous Fibrous Materials Related to Permeability, Diffusivity and Thermal Conductivity. *Fractals* **2017**, *25*, 1750030. [CrossRef]
5. Shafieian, A.; Khiadani, M.; Nosrati, A. A review of latest developments, progress, and applications of heat pipe solar collectors. *Renew. Sustain. Energy Rev.* **2018**, *95*, 273–304. [CrossRef]
6. Phiraphat, S.; Prommas, R.; Puangsombut, W. Experimental study of natural convection in PV roof solar collector. *Int. Commun. Heat Mass Transf.* **2017**, *89*, 31–38. [CrossRef]
7. Liang, M.; Liu, Y.; Xiao, B.; Yang, S.; Wang, Z.; Han, H. An analytical model for the transverse permeability of gas diffusion layer with electrical double layer effects in proton exchange membrane fuel cells. *Int. J. Hydrogen Energy* **2018**, *43*, 17880–17888. [CrossRef]
8. Long, G.; Liu, S.; Xu, G.; Wong, S.; Chen, H.; Xiao, B. A Perforation-Erosion Model for Hydraulic-Fracturing Applications. *SPE Prod. Oper.* **2018**, *33*, 770–783. [CrossRef]

9. Long, G.; Xu, G. The Effects of Perforation Erosion on Practical Hydraulic-Fracturing Applications. *SPE J.* **2017**, *22*, 645–659. [CrossRef]
10. Mey, G.D.; Torzewicz, T.; Kawka, P.; Czerwoniec, A.; Janicki, M.; Napieralski, A. Analysis of nonlinear heat exchange phenomena in natural convection cooled electronic systems. *Microelectron. Reliab.* **2016**, *67*, 15–20. [CrossRef]
11. Purusothaman, A. Investigation of natural convection heat transfer performance of the QFN-PCB electronic module by using nanofluid for power electronics cooling applications. *Adv. Powder Technol.* **2018**, *29*, 996–1004. [CrossRef]
12. Choi, S.U.S.; Eastman, J.A. Enhancing thermal conductivity of fluids with nanoparticles. In Proceedings of the ASME International Mechanical Engineering Congress & Exposition, San Francisco, CA, USA, 12–17 November 1995.
13. Khanafer, K.; Vafai, K.; Lightstone, M. Bouyancy driven heat transfer enhancement in a two dimensional enclosure utilizing nanofluids. *Int. J. Heat Mass Transf.* **2003**, *46*, 3639–3653. [CrossRef]
14. Khanafer, K.; Vafai, K. A critical synthesis of thermosphysical characteristics of nanofluids. *Int. J. Heat Mass Transf.* **2011**, *54*, 4410–4428. [CrossRef]
15. Boungioron, J. Convective transport in nanofluids. *ASME J. Heat Transf.* **2006**, *128*, 240–250. [CrossRef]
16. Oztop, H.F.; Abu-Nada, E. Numerical study of natural convection in partially heated rectangular enclosures filled with nanofluids. *Int. J. Heat Fluid Flow* **2008**, *29*, 1326–1336. [CrossRef]
17. Ghasemi, B.; Aminossadati, S.M.; Raisi, A. Magnetic field effect on natural convection in a nanofluid-filled square enclosure. *Int. J. Therm. Sci.* **2011**, *50*, 1748–1756. [CrossRef]
18. Kefayati, G.H.R.; Hosseinizadeh, S.F.; Gorji, M.; Sajjadi, H. Lattice Boltzmann simulation of natural convection in tall enclosures using water/SiO_2 nanofluid. *Int. Commun. Heat Mass Transf.* **2011**, *38*, 798–805. [CrossRef]
19. Kefayati, G.H.R. Heat transfer and entropy generation of natural convection on non-Newtonian nanofluids in porous cavity. *Powder Technol.* **2016**, *299*, 127–149. [CrossRef]
20. Al-Kouz, W.; Alshare, A.; Kiwan, S.; Al-Muhtady, A.; Alkhalidi, A. Two-dimensional analysis of low-pressure flows in an inclined square cavity with two fins attached to the hot wall. *Int. J. Therm. Sci.* **2018**, *126*, 181–193. [CrossRef]
21. Al-Kouz, W.; Kiwan, S.; Alkhalidi, A.; Sari, M.; Alshare, A. Numerical study of heat transfer enhancement for low-pressure flows in a square cavity with two fins attached to the hot wall using AL_2O_3-air nanofluid. *J. Mech. Eng.* **2018**, *64*, 26–36.
22. Kefayati, G.H.R.; Che Sidik, N.A. Simulation of natural convection and entropy generation of non-Newtonian nanofluid in an inclined cavity using Buongiorno's mathematical model (Part II, entropy generation). *Powder Technol.* **2017**, *305*, 679–703. [CrossRef]
23. Parvin, S.; Chamkha, A.J. An analysis on free convection flow, heat transfer and entropy generation in an odd-shapped cavity filled with nanofluid. *Int. Commun. Heat Mass Transf.* **2014**, *54*, 8–17. [CrossRef]
24. Mejri, I.; Mahmoudi, A.; Abbasi, M.A.; Omri, A. Magnetic field effect on entropy generation in a nanofluid-filled enclosure with sinusoidal heating on both side walls. *Powder Technol.* **2014**, *266*, 340–353. [CrossRef]
25. Mahmoudi, A.; Mejri, I.; Abbasi, M.A.; Omri, A. Analysis of the entropy generation in nanofluid-filled cavity in the presence of magnetic field and uniform heat generation/absorption. *J. Mol. Liq.* **2014**, *198*, 63–77. [CrossRef]
26. Armaghani, T.; Kasaeipoor, A.; Alavi, N.; Rashidi, M.M. Numerical investigation of water-alumina nanofluid natural convection heat transfer and entropy generation in a baffled L-shaped cavity. *J. Mol. Liq.* **2016**, *223*, 243–251. [CrossRef]
27. Al-Zamily, A.M.J. Analysis of natural convection and entropy generation in a cavity filled with multi-layers of porous medium and nanofluid with a heat generation. *Int. J. Heat Mass Transf.* **2017**, *106*, 1218–1231. [CrossRef]
28. Bouchoucha, A.E.M.; Bessaïh, R.; Oztop, H.F.; Al-Salem, K.; Bayrak, F. Natural convection and entropy generation in a nanofluid filled cavity with thick bottom wall: Effect of non-isothermal heating. *Int. J. Mech. Sci.* **2017**, *126*, 95–105. [CrossRef]
29. Ashorynejad, H.R.; Hoseinpour, B. Investigation of different nanofluids effect on entropy generation on natural convection in porous cavity. *Eur. J. Mech. B/Fluids* **2017**, *62*, 86–93. [CrossRef]

30. Sheremet, M.A.; Grosan, T.; Pop, I. Natural convection and entropy generation in a square cavity with variable temperature side walls filled with a nanofluid: Buongiorno's mathematical model. *Entropy* **2017**, *19*, 337. [CrossRef]
31. Alsabery, A.I.; Ishak, M.S.; Chamkha, A.J.; Hashim, I. Entropy Generation analysis and natural convection in a nanofluid-filled square cavity with a concentric solid insert and different temperature distributions. *Entropy* **2018**, *20*, 336. [CrossRef]
32. Siavashi, M.; Yousofvand, R.; Rezanejad, S. Nanofluid and porous fins effect on natural convection and entropy generation of flow inside a cavity. *Adv. Powder Technol.* **2018**, *29*, 142–156. [CrossRef]
33. Kashyap, D.; Dass, A.K. Two-phase lattice Boltzmann simulation of natural convection in a Cu-water nanofluid filled porous cavity: Effects of thermal boundary conditions on heat transfer and entropy generation. *Adv. Powder Technol.* **2018**, *29*, 2707–2724. [CrossRef]
34. Gibanov, N.S.; Sheremet, M.A.; Oztop, H.F.; Abu-Hamdeh, N. Mixed convection with entropy generation of nanofluid in a lid-driven cavity under the effects of a heat-conducting solid wall and vertical temperature gradient. *Eur. J. Mech. B Fluids* **2018**, *70*, 148–159. [CrossRef]
35. Mansour, M.A.; Siddiqa, S.; Gorla, R.S.R.; Rashad, A.M. Effect of heat source and sink on entropy generation and MHD natural convection of Al_2O_3-Cu/water hybrid nanofluid filled with square porous cavity. *Therm. Sci. Eng. Prog.* **2018**, *6*, 57–71. [CrossRef]
36. Rahimi, A.; Sepehr, M.; Lariche, M.J.; Kasaeipoor, A.; Malekshah, E.H. Entropy generation analysis and heatline visualization of free convection in nanofluid (KKL model-based)—Filled cavity including internal active fins using lattice Boltzmann method. *Comput. Math. Appl.* **2018**, *75*, 1814–1830. [CrossRef]
37. Rashidi, M.M.; Nasiri, M.; Shadloo, M.S.; Yang, Z. Entropy Generation in a Circular Tube Heat Exchanger Using Nanofluids: Effects of Different Modeling Approaches. *Heat Transf. Eng.* **2016**, *38*, 853–866. [CrossRef]
38. Yarmand, H.; Ahmadi, G.; Gharehkhani, S.; Kazi, S.; Safaei, M.; Alehashem, M.; Mahat, A. Entropy Generation during Turbulent Flow of Zirconia-water and Other Nanofluids in a Square Cross Section Tube with a Constant Heat Flux. *Entropy* **2014**, *16*, 6116–6132. [CrossRef]
39. Jamalabadi, M.A.; Safaei, M.; Alrashed, A.; Nguyen, T.; Filho, E.B. Entropy Generation in Thermal Radiative Loading of Structures with Distinct Heaters. *Entropy* **2017**, *19*, 506. [CrossRef]
40. Aghaei, A.; Sheikhzadeh, G.A.; Goodarzi, M.; Hasani, H.; Damirchi, H.; Afrand, M. Effect of horizontal and vertical elliptic baffles inside an enclosure on the mixed convection of a MWCNTs-water nanofluid and its entropy generation. *Eur. Phys. J. Plus* **2018**, *133*, 486. [CrossRef]
41. Mahmoudinezhad, S.; Rezania, A.; Yousefi, T.; Shadloo, M.S.; Rosendahl, L.A. Adiabatic partition effect on natural convection heat transfer inside a square cavity: Experimental and numerical studies. *Heat Mass Transf.* **2017**, *54*, 291–304. [CrossRef]
42. Nasiri, H.; Jamalabadi, M.Y.; Sadeghi, R.; Safaei, M.R.; Nguyen, T.K.; Shadloo, M.S. A smoothed particle hydrodynamics approach for numerical simulation of nano-fluid flows. *J. Therm. Anal. Calorim.* **2018**. [CrossRef]
43. Karniadakis, G.; Beskok, A.; Aluru, N. *Microflows and Nanoflows*; Springer: Berlin, Germany, 2005.
44. Lockerby, D.; Reese, J.; Barber, R. Velocity boundary condition at solid wall in rarefied gas calculations. *Phys. Rev. E* **2004**, *70*, 017303. [CrossRef] [PubMed]
45. Colin, S. *Heat Transfer and Fluid Flow in Minichannels and Microchannels: Single-Phase Gas Flow in Microchannels*; Elsevier: Amsterdam, The Netherlands, 2006.
46. Versteeg, H.; Malalasekera, W. *An Introduction to Computational Fluid Dynamics: The Finite Volume Method*; Prentice-Hall: Upper Saddle River, NJ, USA, 1995.
47. Patankar, S.V.; Spalding, D.B. A calculation procedure for heat, mass and momentum transfer in three-dimensional parabolic flows. *Int. J. Heat Mass Transf.* **1972**, *15*, 1787–1806. [CrossRef]